Quantum Dots Hot Paper

How to cite: *Angew. Chem. Int. Ed.* **2022,** *61,* e202214177
International Edition: doi.org/10.1002/anie.202214177
German Edition: doi.org/10.1002/ange.202214177

Spatially Directed Biosynthesis of Quantum Dots via Spidroin Templating in *Escherichia coli*

Meng-Ting Chen[+], Chun-Fei Hu[+], Hai-Bo Huang, Zhi-Gang Qian, and Xiao-Xia Xia**

Abstract: Spatially directed synthesis of quantum dots (QDs) is intriguing yet challenging in organisms, due to the dispersed feature of templating biomolecules and precursors. Whether this task could be accomplished by biomolecular condensates, an emerging type of membraneless compartments in cells remains unknown. Here we report synthetic protein condensates for templated synthesis of QDs in bacterium *Escherichia coli.* This was realized by overexpression of spider silk protein to bind precursor ions and recruit other necessary components, which induced the spidroin to form more β-sheet structures for assembly and maturation of the protein condensates. This in turn enabled formation and co-localization of the fluorescent QDs to "light up" the condensates, and alleviated cytotoxicity of the precursor heavy metal ions and resulting QDs. Thus, our results suggest a new strategy for nanostructure synthesis and deposition in subcellular compartments with great potential for in situ applications.

Introduction

Quantum dots (QDs) are nanometer-size semiconducting particles that possess unique size- and shape-dependent optical and optoelectronic properties.[1,2] Their structural stability, high brightness, resistance to photobleaching and multiplexing capacity make QDs excellent candidates for biosensing and imaging.[1,3] Biosynthesis of QDs is a promising strategy because it not only carries out the synthetic reactions under environmentally friendly conditions, but also endows the QDs with biostability and biocompatibility.[4–6] In particular, formation of QDs in living microorganisms such as bacterial, fungal, and mammalian cells has shown great promise for implementation.[7–10] Their natural abilities to produce a variety of sophisticated nanostructures are attributed to the rich sources of redox enzymes, metal binding domains and certain biochemicals within the cells. This has in turn inspired overexpression of the redox enzymes and elevation in the intracellular pools of the involved biochemicals to tune the QDs formation.[6,11–13] However, due to the intrinsic dispersed feature of these enzymes and biochemicals within the natural and engineered production hosts, biosynthesis of QDs in a spatially directed manner remains elusive in living cells.

Unlike traditional membrane-bound organelles, biomolecular condensates are subcellular membranless compartments formed by liquid-liquid phase separation (LLPS) of scaffolding proteins.[14–16] These scaffolding proteins share common features in that they are typically composed of intrinsically disordered regions with low-complexity sequences, which are characterized by long stretches with a low overrall diversity of amino acid residues rich in glycine and serine.[14,17] These features facilitate the scaffolding proteins to form liquid droplets and protein-rich condensates via intermolecular interactions such as cation-π, hydrophobic, and electrostatic interactions.[18] We surmise that biomolecular condensates might template QDs formation in a spatial manner within living cells due to the following three reasons. First, it is increasingly recognized that condensation of the scaffolding proteins typically proceeds by nucleation and growth, and these scaffolding proteins undergoing LLPS might have great potential to aid nucleation and growth of QDs. Second, the concentrated feature of the biomolecular condensates is highly desirable for accelerating QDs formation under the physiologically benign conditions. Finally, the in situ formed QDs may be well localized and stabilized within the biomolecular condensates which contributes to protect the nascent QDs from aggregation and fluorescence quenching.

In this study, we investigated the hypothesis that synthetic protein condensates in cells might template the formation and co-localization of the resulting QDs. To search for suitable templating condensates, we generated three series of synthetic protein condensates from intrinsically disordered proteins (type I and type II spider silk proteins, and resilin-like proteins) in the model prokaryotic cells of bacterium *Escherichia coli.* Then we evaluated the capabilities of these condensates for the spatially directed biosynthesis, and revealed the key feature critical for the directed synthesis, which was specific to the silk proteins due to their instinct propensity to form β-sheet secondary structures. Furthermore, we demonstrated the beneficial outcome of the compartmentalized biosynthesis for the bacterial cells.

[*] M.-T. Chen,[+] C.-F. Hu,[+] H.-B. Huang, Prof. Z.-G. Qian, Prof. X.-X. Xia
State Key Laboratory of Microbial Metabolism, Joint International Research Laboratory of Metabolic & Developmental Sciences, School of Life Sciences and Biotechnology, Shanghai Jiao Tong University, 800 Dongchuan Road, Shanghai 200240 (China)
E-mail: zgqian@sjtu.edu.cn
xiaoxiaxia@sjtu.edu.cn

[+] These authors contributed equally to this work.

Results and Discussion

We started our intestication by recominantly overexpressing spider dragline silk proteins to form synthetic condensates in the model bacterium *E. coli* as demonstrated in our recent study.[19] As the molecular weight of scaffolding proteins would affect multivalent interactions between protein chains and their LLPS behavior,[20] initially we made three silk protein constructs for their overexpression. These silk proteins were composed of 8, 16, and 32 consensus units of the central repetitive domain of the major ampullate spidroin 1 of the spider *Trichonephila clavipes*, and hereafter termed I8, I16, and I32, respectively. As expected, all the three overexpressed silk proteins formed subcellular condensates near the cell pole regions, whereas such condensates were absent in the control cells (Figure S1a).

Then we studied whether the silk protein condensates would support compartmentalized QDs formation within the living *E. coli* cells. As a typical example, here we intended to biosynthesize CdSe QDs due to their excellent optical characteristics and great potential for subcellular imaging.[21,22] To this end, the silk protein-expressing cells were exposed to $CdCl_2$ and Na_2SeO_3 and analyzed at 4 h post-treatment. Confocal imaging revealed formation of fluorescent QDs that were spatially localized near the pole regions of silk protein-expressing cells (Figure 1a), whereas the control cells without silk could barely support the biogenesis of fluorescent QDs. Further cell fluorescence analysis revealed that the silk protein I16-expressing cells produced the highest level of QDs fluorescence signal (Figure 1b). In addition, the fluorescence lifetime of the QDs synthesized by the I16-expressing cells was appreciably high at 65 ns, which was superior to those synthesized by the silk protein I8- and I32-expressing cells (Figure 1c; Figure S2). These differences in QDs biosynthesis might not be due to the variations in silk protein concentration within the cells because the three silk proteins were expressed at comparable levels (Figure S3). Instead, this might be correlated with the moderate capability of I16 to form β-sheet structures beneficial for the nucleation and growth of the QDs within the cells (Figure S4).

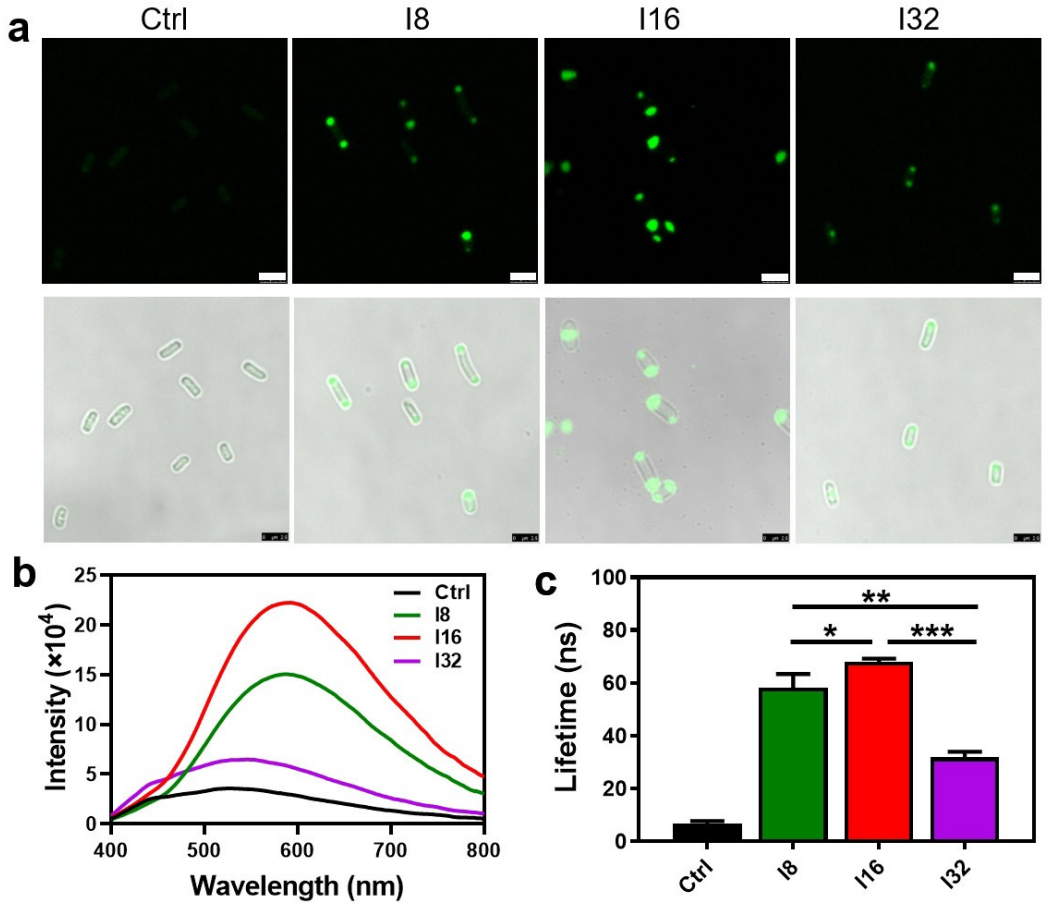

Figure 1. Spatially directed formation of QDs in silk protein-expressing *E. coli* cells. a) Fluorescence microscopy (upper) and merged bright-field and fluorescent images (lower) of the silk protein-expressing cells treated with1 mM $CdCl_2$ and Na_2SeO_3. The cells harboring empty vector were similarly excited at 405 nm, and emited background level of fluorescence serving as a control. Scale bar: 2.5 μm. b) Fluorescence emission spectra of the control and silk protein-expressing cells at 350 nm excitation. c) Fluorescence lifetime of the biogenic QDs from the respective *E. coli* cells. Data in c are presented as mean ± s.d. of $n = 3$ samples. Statistical significance was determined using one-way analysis of variance (ANOVA) for P values (*$P < 0.05$; **$P < 0.01$; ***$P < 0.001$).

We also studied whether similar QDs could be synthesized in condensates derived from other IDPs, such as type II spider dragline silk proteins (similar to the type I silk proteins in the formation of β-sheet structures) and resilin-like proteins which could not form β-sheets. These two series of proteins have different amino acid sequences from the type I silk proteins (Table S1), and also formed condensates upon overexpression in *E. coli* (Figure S1b and S1c). Interestingly, the type II silk protein II8 enabled QDs formation but the resilin-like proteins did not (Figure S5), indicating that the spatially directed biosynthesis might be specific to the spidroins. As previously demonstrated, the β-sheet structures of other peptide and protein templates played a vital role to modulate nanostructure formation in vitro.[23–25] Taken together, our results indicated that the silk protein length was critical in determining the fluorescence intensity and lifetime of the spatially formed QDs.

Next we focused on identifying the QDs synthesized by the silk protein I16-expressing cells. Interestingly, elemental mapping revealed enrichment of the Cd, Se and S elements near the cell pole regions, which overlapped with the silk protein condensates imaged by bright-field transmission electron microscopy (TEM) and high-angle annular dark-field scanning transmission electron microscopy (HAADF-STEM) (Figure 2a). Instead we observed enrichment of Cd and Se (rather than S) elements in the control cells to form intracellular precipitates with irregular morphologies by the HAADF imaging, yet these precipitates were not observed in the bright-field imaging mode (Figure 2b). Quantification of atomic fractions revealed that the Cd, Se, and S elements in the condensates were over twofold higher than those of the bulk phase (Figure 2c). In addition, the Cd fraction in the condensates was almost equal to the sum of Se and S fractions, leading us to propose the composition of the QDs as $CdSe_XS_{1-X}$ other than previously expected CdSe QDs. This was possibly attributed to the involvement of certain reducing agents (such as cysteine) in the biosynthesis of the $CdSe_XS_{1-X}$ QDs (see reconstitution assay below). In contrast, the control cells could only generate Cd- and Se-rich precipitates (Figure 2d), which barely fluoresced inside the living cells (Figure 1a), possibly due to fluorescence quenching resulting from QDs aggregation.[26] Again, these results stressed the silk protein I16 was critical for the formation and co-localization of the fluorescent $CdSe_XS_{1-X}$ QDs within the protein condensates.

We further characterized the $CdSe_XS_{1-X}$ QDs by lysing the I16-expressing cells. The resulting cell lysate was clear and homogeneous, and emitted bright yellow fluorescence under UV-irradiation, whereas the lysate from the control cells did not fluoresce (Figure S6a). Fluorescence excitation-emission matrix spectroscopy on the yellow fluorophore showed a maximum at ≈575 nm emission under 350 nm

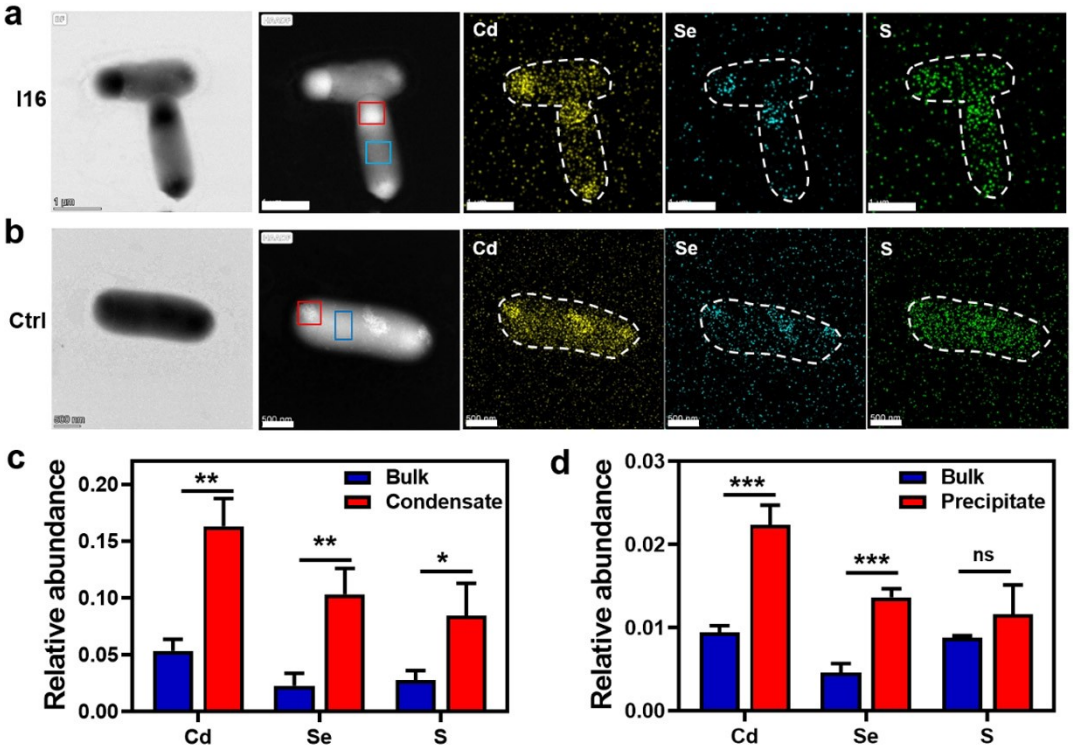

Figure 2. Formation and co-localization of $CdSe_XS_{1-X}$ QDs within the silk protein condensates. TEM images and elemental mapping of a) silk protein I16-expressing and b) control cells. The cells were treated with 0.1 mM IPTG for 2 h, and then exposed to 1 mM $CdCl_2$ and Na_2SeO_3 for 4 h to allow spatially defined formation of the QDs. Scale bars in a, 1 μm; scale bars in b, 0.5 μm. Relative abundance of Cd, Se and S elements within and outside the condensates in the I16-expressing cells (c), and within and outside the presipitates in the control cells (d). The selected boxes in panel a and b indicate the respective subcellular loci. Data in c and d are presented as mean ± s.d. of $n = 3$ samples. Statistical significance was determined using one-way ANOVA (ns, not significant with $P > 0.05$; *$P < 0.05$; **$P < 0.01$; ***$P < 0.001$).

excitation (Figure S6b). UV/Vis absorption spectroscopy showed the absorption peak at ≈420 nm with ≈50 nm peak width (Figure S6c), which was in accordance with the absorption spectra for $CdSe_XS_{1-X}$ QDs.[11] The full width at half maximum (FWHM) of our spatially synthesized $CdSe_XS_{1-X}$ QDs was about 192 nm, which is moderately higher than the value (140 nm) typically reported by microbial synthesis and demonstrated with good potential for in vivo imaging applications.[11] Notably, the FWHM of our QDs could be further tuned by the approaches previously proposed for biosynthesis,[8,13] such as engineering the protein templates, adjusting metal ion concentrations, and duration time of the co-incubation of the cells with metal ions. In addition, our $CdSe_XS_{1-X}$ QDs biosynthesized in the I16 condensates had a quantum yield of 3.09%, which is comparable to the previously reported values by microbial synthesis (Table S2). Further size distribution analysis revealed that our QDs had an average diameter of 1.66 ± 0.35 nm (Figure S7a), and the crystal-lattice distance was determined to be 0.349 nm (Figure S7b), which was comparable with those reported previously.[11,13] In addition, the presence of Se, Cd, and S elements in our $CdSe_XS_{1-X}$ QDs was verified by energy-dispersive X-ray spectroscopy (Figure S7c).

To elucidate the templating role of silk protein in $CdSe_XS_{1-X}$ QDs genesis, in vitro reconstitution of QDs biosynthesis was performed using purified silk protein I16. To this end, $CdCl_2$, Na_2SeO_3, and cysteine (a reducing agent natively produced by *E. coli*) was reconstituted into a physiologically relevant buffer supplemented with the silk protein at a range of concentrations. The mixtures were then incubated at 30 °C for 30 min for the formation of QDs. Fluorescence analysis revealed characteristic fluorescence emission at ≈580 nm from I16-containing reaction mixtures (Figure S8), which was analogous to the QDs synthesized within the intact cells, whereas the characteristic fluorescence signal was undetectable from the control reaction without the silk protein. We also observed slight blue shift of the fluorescence emission when the silk protein concentration was increased from 5 to 25 mg mL^{-1}, which might be associated with the biosynthesis of QDs with smaller sizes. These results demonstrated the critical templating role of the silk protein in the biosynthesis of the $CdSe_XS_{1-X}$ QDs.

For more details on how the silk protein templated the formation and subcellular co-localization of the $CdSe_XS_{1-X}$ QDs, we monitored the silk protein structures in the *E. coli* cells. As β-sheet secondary structures are prevalent in natural spider dragline silk,[27–29] we reasoned that such structures might also exist in the silk protein-expressing *E. coli* cells. Therefore, Thioflavin T (ThT), a cell-permeable fluorescent dye that probes the β-sheet-rich structures,[30] was used to stain the cells for fluorescence imaging. Notably, we observed a moderate increase in the cell fluorescence when the control cells were treated with the precursor heavy metal ion Cd^{2+} (Figure 3a), indicating that Cd^{2+} could bind and induce certain endogenous proteins of *E. coli* to form more β-sheet secondary structures as demonstrated in the in vitro reconstitution study (Figure S9). This binding may adversely affect the physiological functions of those endogenous proteins, and exert a cytotoxic effect on the bacterial cells (see growth retardation results below). More interestingly, treating the silk protein I16-expressing cells with Cd^{2+} resulted in a drastically higher cell fluorescence, and clearer compartmentalization of the silk protein condensates as compared to the nontreated cells. This proved that Cd^{2+}-induced formation of β-sheet structures would facitalite intermolecular interactions of the silk protein to form mature condensates, possibly by coordination and/or electrostatic binding of the Cd^{2+} ion to specific amino acid residues of the silk protein. When these cells were additionally treated with SeO_3^{2-} for QDs formation, the silk protein condensates were well retained in spite of the fact that the overall ThT fluorescence of the cells was significantly reduced. A possible explanation was that the $CdSe_XS_{1-X}$ QDs formation and co-localization partially relieved the inducing effect of Cd^{2+} on β-sheet formation (Figure 3b). Furthermore, these observations on silk protein structure transition upon Cd^{2+} treatment and $CdSe_XS_{1-X}$ QDs formation were recapitulated by in vitro reconstitution using the purified silk protein I16 (Figure S10).

Futhermore, we explored whether the spatically directed biosynthesis of the $CdSe_XS_{1-X}$ QDs would benifit the fitness of the bacterial production host. To this end, we monitored the biomass (optical density at 600 nm) of the *E. coli* cells before and after the QDs formation (Figure 3c). Not surprisingly, the control cells without silk protein underwent a growth retardation upon the Cd^{2+} ion treatments, either alone or in combination with SeO_3^{2-}, clearing demonstrating the cytotoxicity of the heavy metal ion on the bacterium.[31,32] This coincided with the above observation on Cd^{2+}-induced β-sheet formation from the bacterial endogenous proteins leading to deterioration of certain cellular activities responsible for cell growth. In contrast, formation and co-localization of the $CdSe_XS_{1-X}$ QDs enabled the silk protein-expressing cells to fully recover the growth fitness, which would otherwise be deteriorated by the Cd^{2+} treatment alone. This might be explained by that the critcial cellular activities recovered their physiological functions for normal cell growth when the toxic Cd^{2+} ions were converted into $CdSe_XS_{1-X}$ QDs and deposited into the silk protein condensates. These results indicated that the silk protein condensates would protect the bacterial host from abnormal protein structural transformation and alleviate the cytotoxicity of the precursor metal ion and the resulting QDs.

Having found recovery of bacterial fitness upon $CdSe_XS_{1-X}$ QDs biogenesis and compartmentalized co-localization, we were curious about whether the silk protein could preferentially bind Cd^{2+} for detoxification in the protein condensates. Therefore, the silk protein I16-expressing cells were treated with Cd^{2+} alone (this experiment differs from that presented in Figure 2) and analyzed by TEM and elemental imaging. We found that the silk protein condensates were enriched with both Cd and S elements (Figure 4a), whereas such enrichments were not observed in the silk protein condensates without Cd^{2+} treatment or the control cells without the silk protein (Figure S11). Quantification of the atomic fractions revealed that the Cd and S

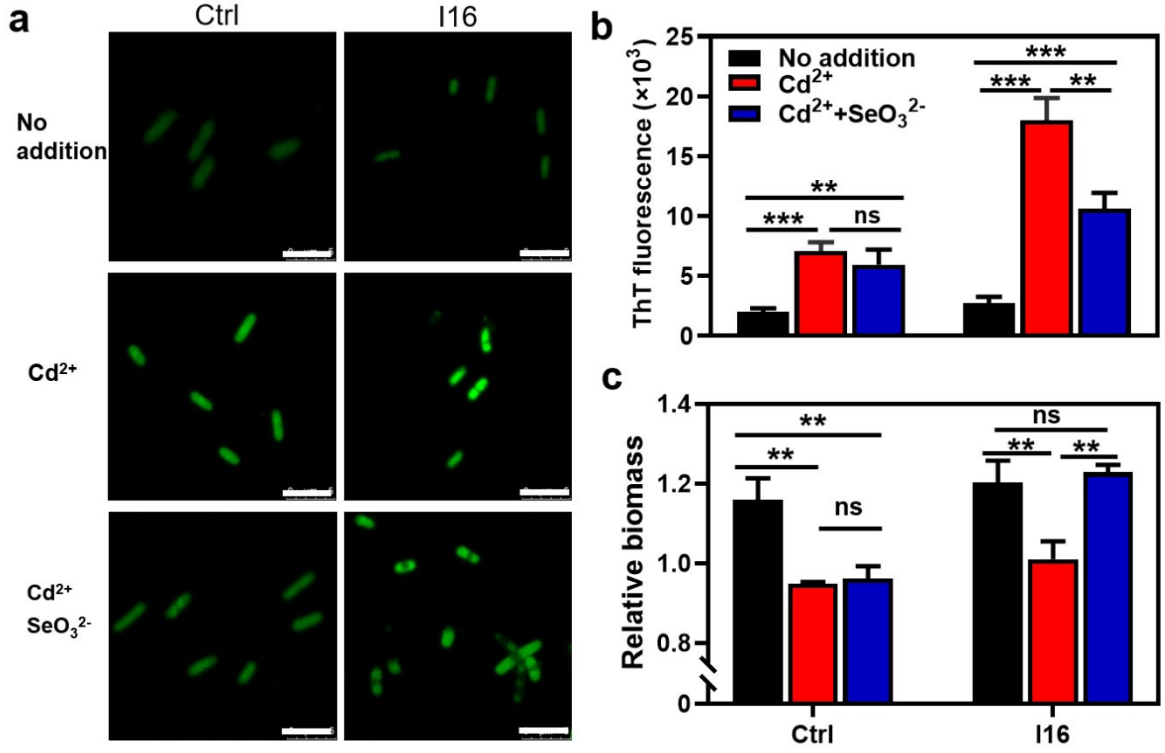

Figure 3. Recovery of bacterial fitness upon QDs biogenesis and co-localication in the synthetic protein condensates. a) Fluorescence microscopy images of the control and I16-expressing *E. coli* cells without and with treament of Cd^{2+} alone or in combination with SeO_3^{2-}. The cells were stained with ThT, a fluorescent probe to detect β-sheet structures, and excited at 458 nm. Scale bars: 5 μm. b) Fluorescence intensity at 490 nm of the ThT-stained cells. c) Effect of ion treatment on the cell growth. The ratio of cell biomass 4 h after the ion treatment to that just before the treatment was calculated and shown. Data in b and c are presented as mean ± s.d. of $n = 3$ samples. Statistical significance was determined using one-way ANOVA (ns, not significant with $P > 0.05$; $^{**}P < 0.01$; $^{***}P < 0.001$).

elemental fractions in the silk protein condensates were over threefold higher than those in the bulk phase of the cells (Figure 4b). A closer inspection of the condensates revealed that the S fraction was approximately twofold higher than that of the Cd element, which is inspiring and consistent with the coordination ratio of a cadmium ion to a thiol group.[33] It is reasoned that the enrichment of S element should be an outcome of the Cd^{2+} enrichment in the silk protein condensates. Therefore, these results suggested a possible detoxification mechanism acquired by the *E. coli* cells to preferentially bind Cd^{2+} and recruit sulfur-containing reducing agents within the silk protein condensates.

Based on the above observations, here we propose a model for the spatially directed biosynthesis and localization of $CdSe_XS_{1-X}$ QDs within the silk protein condensates of bacterium *E. coli* (Scheme 1). When the silk protein-expressing cells were exposed to the Cd^{2+} ion, permeation of the heavy metal ion into the cytoplasmic milieu of the bacterium allowed its binding to the recombinant silk protein. This binding induced the silk protein to form more β-sheet secondary structures facilitating intermolecular interactions (such as hydrogen bonding) of the silk protein to undergo LLPS. The binding of Cd^{2+} also enabled the silk protein to coordinate and enrich thiol-containing agents such as cysteine, glutathione and/or other more complex reductants. In particular, the uptake of SeO_3^{2-} and binding

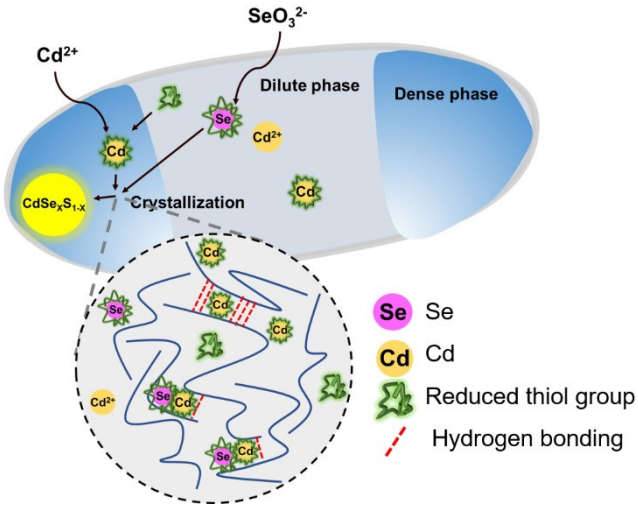

Scheme 1. Schematic diagram of spatially directed biosynthesis and localization of $CdSe_XS_{1-X}$ QDs within the subcellular silk protein condensates.

with certain thiol-containing molecules might also be recruited into the Cd^{2+}-silk protein complex to trigger crystallization and growth of the $CdSe_XS_{1-X}$ QDs. With the nascent QDs co-localized within the silk condensates in situ,

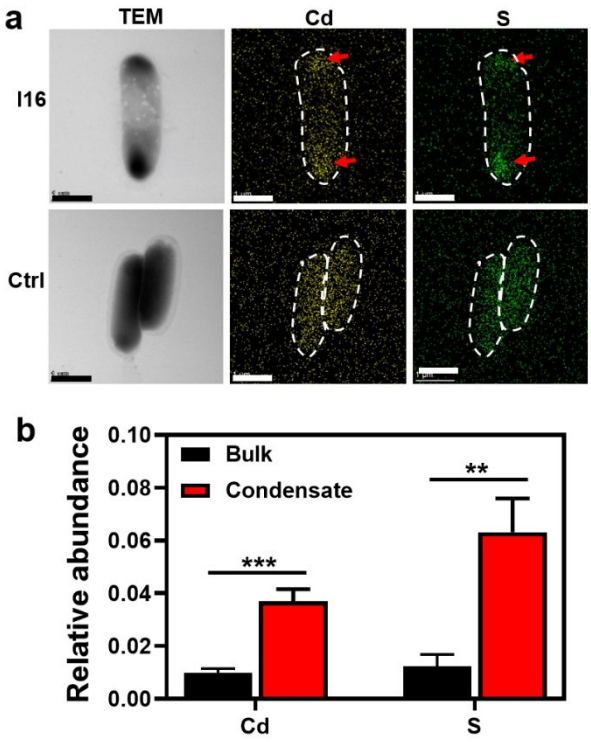

Figure 4. Preferential binding of Cd^{2+} and recruitment of sulfur containing agents within the silk protein I16 condensates. a) TEM images and elemental mapping of the silk protein I16-expressing and control cells treated with Cd^{2+}. The red arrows indicate the positions of the silk protein condensates. b) Relative abundance of Cd and S elements within and outside the condensates of the I16-expressing cells with Cd^{2+} treatment. Data in b are presented as mean ± s.d. of $n = 3$ samples. Statistical significance was determined using one-way ANOVA (**$P < 0.01$; ***$P < 0.001$).

this spatially defined and templated dispersion of the QDs contributes to reduce their precipitation, and drives the biosynthesis reaction to alleviate the cytotoxicity of the precursor heavy metal ion and the resulting QDs on the bacterium.

Conclusion

In this work we have demonstrated a new strategy for spatially directed synthesis of QDs in living cells of the model bacterium *E. coli*. This is achieved by relying on a unique member of a family of intrinsically disordered proteins that could autonomously assemble biomolecular condensates. The recombinant spider dragline silk protein may play dual roles in the *E. coli* cells: first, the silk protein templates QDs biosynthesis by binding precursor metal ion, recruiting endogenous reducing agents and other necessary components, and undergoing secondary structural transitions to aid crystallization and growth of the QDs; second, the silk protein condensates serve as a hub to disperse and stabilize the nascent QDs via co-localization within the subcellular compartments. In turn, the compartmented formation of QDs in living cells may result in at least two advantages. First, the living cells with silk protein condensates provide concentrated biomolecular template and other necessary components (such as biogenic reducing agents) for QDs biosynthesis in all aqueous solutions at physiological conditions, supporting facile, benign and controllable QDs biosynthesis in situ. Second, subcellular localization and dispersion stabilize the QDs and improve the optical properties such as fluorescence intensity and lifetime, making the compartmented QDs promising for use in subcellular imaging. As the scaffolding proteins of biomolecular condensates share common features, we envision that the new strategy developed here can be taken for spatially directed formation of QDs with diverse optical, physical and chemical properties in other prokaryotic and eukaryotic cells for broad applications. In particular, the strategy is expected to be applicable for the compartmentalized biosynthesis of other QDs and semiconductor materials with more sophisticated core–shell structures.[34,35] To this end, engineering the physiochemical properties of the protein condensates, programming the addition of diverse precursor ions, and/or optimizing the cell culture conditions should be necessary to improve their metal binding and reduction capabilities, and such systematic studies are underway in our laboratory.

Acknowledgements

Financial support was provided by the National Key Research and Development Program of China (Grant Nos. 2021YFA0909502 and 2020YFA0907702), the National Natural Science Foundation of China (Grant Nos. 32270107, 32071414, and 22075179), and the Natural Science Foundation of Shanghai (21ZR1432100).

Conflict of Interest

The authors declare no conflict of interest.

Data Availability Statement

The data that support the findings of this study are available in the Supporting Information of this article.

Keywords: Biomolecular Condensate · Membraneless Compartment · Quantum Dots · Spider Dragline Silk Protein · Synthetic Biology

[1] A. L. Efros, J. B. Delehanty, A. L. Huston, I. L. Medintz, M. Barbic, T. D. Harris, *Nat. Nanotechnol.* **2018**, *13*, 278–288.
[2] D. V. Talapin, A. L. Rogach, A. Kornowski, M. Haase, H. Weller, *Nano Lett.* **2001**, *1*, 207–211.
[3] K. D. Wegner, N. Hildebrandt, *Chem. Soc. Rev.* **2015**, *44*, 4792–4834.
[4] Y. Choi, S. Y. Lee, *Nat. Chem. Rev.* **2020**, *4*, 638–656.
[5] L. J. Tian, W. W. Li, T. T. Zhu, J. J. Chen, W. K. Wang, P. F. An, L. Zhang, J. C. Dong, Y. Guan, D. F. Liu, N. Q. Zhou, G.

Liu, Y. C. Tian, H. Q. Yu, *J. Am. Chem. Soc.* **2017**, *139*, 12149–12152.
[6] Y. Choi, T. J. Park, D. C. Lee, S. Y. Lee, *Proc. Natl. Acad. Sci. USA* **2018**, *115*, 5944–5949.
[7] K. L. Naughton, J. Q. Boedicker, *ACS Synth. Biol.* **2021**, *10*, 3475–3488.
[8] R. Cui, H. H. Liu, H. Y. Xie, Z. L. Zhang, Y. R. Yang, D. W. Pang, Z. X. Xie, B. B. Chen, B. Hu, P. Shen, *Adv. Funct. Mater.* **2009**, *19*, 2359–2364.
[9] S. R. Stürzenbaum, M. Hoeckner, *Nat. Nanotechnol.* **2013**, *8*, 57–60.
[10] L. H. Xiong, J. W. Tu, *Sci. China Chem.* **2020**, *63*, 448–453.
[11] L. J. Tian, Y. Min, W. W. Li, J. J. Chen, N. Q. Zhou, T. T. Zhu, D. B. Li, J. Y. Ma, P. F. An, L. R. Zheng, H. Huang, Y. Z. Liu, H. Q. Yu, *ACS Nano* **2019**, *13*, 5841–5851.
[12] S. H. Kang, K. N. Bozhilov, N. V. Myung, A. Mulchandani, W. Chen, *Angew. Chem. Int. Ed.* **2008**, *47*, 5186–5189; *Angew. Chem.* **2008**, *120*, 5264–5267.
[13] T. J. Park, S. Y. Lee, N. S. Heo, T. S. Seo, *Angew. Chem. Int. Ed.* **2010**, *49*, 7019–7024; *Angew. Chem.* **2010**, *122*, 7173–7178.
[14] S. Alberti, A. Gladfelter, T. Mittag, *Cell* **2019**, *176*, 419–434.
[15] S. F. Banani, H. O. Lee, A. A. Hyman, M. K. Rosen, *Nat. Rev. Mol. Cell Biol.* **2017**, *18*, 285–298.
[16] D. Bracha, M. T. Walls, C. P. Brangwynne, *Nat. Biotechnol.* **2019**, *37*, 1435–1445.
[17] K. L. Saar, A. S. Morgunov, R. Qi, W. E. Arter, G. Krainer, A. A. Lee, T. P. J. Knowles, *Proc. Natl. Acad. Sci. USA* **2021**, *118*, e2019053118.
[18] Y. Shin, C. P. Brangwynne, *Science* **2017**, *357*, eaaf4382.
[19] S. P. Wei, Z. G. Qian, C. F. Hu, F. Pan, M. T. Chen, S. Y. Lee, X. X. Xia, *Nat. Chem. Biol.* **2020**, *16*, 1143–1148.
[20] B. S. Schuster, E. H. Reed, R. Parthasarathy, C. N. Jahnke, R. M. Caldwell, J. G. Bermudez, H. Ramage, M. C. Good, D. A. Hammer, *Nat. Commun.* **2018**, *9*, 2985.
[21] I. L. Medintz, H. T. Uyeda, E. R. Goldman, H. Mattoussi, *Nat. Mater.* **2005**, *4*, 435–446.
[22] A. M. Wagner, J. M. Knipe, G. Orive, N. A. Peppas, *Acta Biomater.* **2019**, *94*, 44–63.
[23] Y. Feng, H. Wang, J. Zhang, Y. Song, M. Meng, J. Mi, H. Yin, L. Liu, *Biomacromolecules* **2018**, *19*, 2432–2442.
[24] W. Yang, W. Guo, J. Chang, B. Zhang, *J. Mater. Chem. B* **2017**, *5*, 401–417.
[25] O. Deschaume, B. De Roo, M. J. Van Bael, J.-P. Locquet, C. Van Haesendonck, C. Bartic, *Chem. Mater.* **2014**, *26*, 5383–5393.
[26] M. Noh, T. Kim, H. Lee, C. K. Kim, S. W. Joo, K. Lee, *Colloids Surf. A* **2010**, *359*, 39–44.
[27] J. L. Yarger, B. R. Cherry, A. van der Vaart, *Nat. Rev. Mater.* **2018**, *3*, 18008.
[28] C. F. Hu, Z. G. Qian, Q. Peng, Y. Zhang, X. X. Xia, *ACS Biomater. Sci. Eng.* **2021**, *7*, 3608–3617.
[29] Q. Jin, F. Pan, C. F. Hu, S. Y. Lee, X. X. Xia, Z. G. Qian, *Metab. Eng.* **2022**, *70*, 102–114.
[30] M. Biancalana, S. Koide, *Biochim. Biophys. Acta Proteins Proteomics* **2010**, *1804*, 1405–1412.
[31] J. H. Priester, P. K. Stoimenov, R. E. Mielke, S. M. Webb, C. Ehrhardt, J. P. Zhang, G. D. Stucky, P. A. Holden, *Environ. Sci. Technol.* **2009**, *43*, 2589–2594.
[32] D. Cui, J. Wang, H. Wang, Y. Yang, M. Zhao, *J. Hazard. Mater.* **2021**, *409*, 124485.
[33] O. Delalande, H. Desvaux, E. Godat, A. Valleix, C. Junot, J. Labarre, Y. Boulard, *FEBS J.* **2010**, *277*, 5086–5096.
[34] N. Órdenes-Aenishanslins, G. Anziani-Ostuni, C. P. Quezada, R. Espinoza-González, D. Bravo, J. M. Pérez-Donoso, *Front. Microbiol.* **2019**, *10*, 1587.
[35] J. H. Jung, S. Y. Lee, T. S. Seo, *Small* **2018**, *14*, 1803133.

Manuscript received: September 26, 2022
Accepted manuscript online: October 17, 2022
Version of record online: November 10, 2022